BICONICAL TRANSMITTING ANTENNAS, A NUMERICAL ANALYSIS

Vahid Badii*, Ken Tomiyama#, Dale M Grimes
Department of Electrical and Computer Engineering
The Pennsylvania State University
University Park PA 16802

ABSTRACT

We have obtained a general, numerical solution of an ideal biconical transmitting antenna, with arbitrary arm length and conic angle. We evaluate all necessary spherical functions, including Legendre functions of integer and noninteger degrees, spherical Bessel functions of noninteger degrees, and spherical Hankel functions of integer degrees. Using Schelkunoff's solution, field coefficients appear as an infinite set of unknowns that satisfy a linear equation. We truncate the infinite set at 16: for a 5° antenna the Legendre functions have maximum degree 33.3 in the interior region and 31 in the exterior region. To minimize the error, we discard the last two terms in all field, power, and impedance calculations. Solutions are checked in several ways for consistency, including evaluating and comparing calculated fields across the antenna aperture. Results obtained are input impedance, radiation pattern, all fields including near and far ones, and antenna surface current and charge density. Representative plots of all results are included.

* Present address: Department of Engineering
Indiana-Purdue University at Fort Wayne
Fort Wayne, IN 46805

Present address: Mechanical Engineering Department
Aoyama Gakuin University
Setagaya-ku, Tokoyo 157 Japan

INTRODUCTION

Although finite element solutions are available for symmetric radiating and scattering elements, and are both useful and informative, still there are things to be gained from a modal analysis. The presence of an electromagnetically exact solution assures that the full set of needed modes are included. The relative importance of the different higher order modes may be noted; they provide physical meaning for the different radiative units and add to the general knowledge of radiative processes. The result, for this particular case, appears to be a standard against which to measure the accuracy of other, non-exact solutions that are applicable to a much wider variety of radiation problems.

During the decades since Schelkunoff published the first full radiation solution of biconical transmitting antennas (Schelkunoff, 1946) there have been significant further developments. (Schelkunoff, 1952), (Tai, 1948), (Smith, 1948). More recently other, perhaps more readable, analyses were added, (Tai, 1984), (Wait, 1969). Grimes (Grimes, 1982) extended the work to include the full modal scattering solution of biconical receiving antennas with arbitrary loads.

Although the field equations are complete, they have the practical difficulty of being in the form of infinite sums over spherical special functions: functions of fractional or integer degree, respectively, in the interior or exterior antenna region. When the equations were first derived, both they and the functions they contain were so complex that a general numerical evaluation was simply impractical. Only the special cases of extreme cone angles (Schelkunoff, 1946) or fortuitous numerical combinations (Tai, 1949) were evaluated.

Progress both in digital computers and in techniques for

numerical analysis have provided the capability of obtaining a complete and reasonably accurate numeric solution for a biconical antenna over a wide range of sizes. We have obtained such a solution for transmitting antennas.

The method is detailed, then internal checks are applied and discussed. Results obtained include all fields, including near and far ones, from which we obtain the current and charge density on the arms and caps, and the radiated power. Our power plots versus normalized arm length made using the input parameters and again using the far fields are indistinguishable.

BOUNDARY CONDITIONS

The Schelkunoff solution, without loss of generality, makes the z axis the antenna axis, thereby restricting the solution to zero order Legendre functions and their derivatives. The origin of coordinates lies between cone tips, thereby limiting the general solution to odd degree Legendre functions. The geometry is sketched in Figure 1, with Region 1 being the exterior region, Region 2 being the interior region, and Region 3 the source or input. The cone angle is ψ, arm radius is a, and source radius is b. We take b to be vanishingly small.

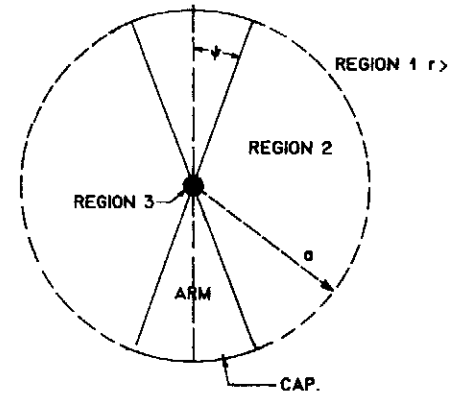

Figure 1. Model of Biconical Antenna used. Cone arm length is "a", and conical half angle is " ψ". Region 3 is a spherical driving point region, centered at the origin. Region 1, the exterior region, is all space at distance r>a. Region 2, the interior region, is with radius b<r<a and angle $\psi < \theta < (\pi - \psi)$.

With r representing the distance from the origin and θ the polar angle, space is divided into three regions:

Region 1. $r > a$.

Region 2. $a > r > b$; $\pi-\psi > \theta > \psi$.

Region 3. $b > r$.

The boundary conditions, with $\sigma=kr$, are:

I $E_\theta \Rightarrow \exp(-i\sigma)/\sigma$ as $r \Rightarrow \infty$

II $H_\phi \Rightarrow \exp(-i\sigma)/\sigma$ as $r \Rightarrow \infty$

III $E_\theta(b,\theta)$ integrable over θ as $b \Rightarrow 0$

IV $H_\phi(b,\theta)$ integrable over θ as $b \Rightarrow 0$

V $E_r(\psi) = E_r(\pi-\psi) = 0$ $b<r<a$

VI $E_r(a^-) = E_r(a^+)$ $\psi<\theta<\pi-\psi$

VII $H_\phi(a^-) = H_\phi(a^+)$ $\psi<\theta<\pi-\psi$

VIII $E_\theta(a^-) = E_\theta(a^+)$ $\psi<\theta<\pi-\psi$

IX $E_\theta(a) = 0$ $0\leq\theta<\psi$; $\pi-\psi<\theta\leq\pi$

REGION 1 FIELDS

A complete description of the fields in Region 1 requires a sum over an infinite set of TM modes. With $e^{j\omega t}$ time dependence, Boundary Conditions I and II require spherical Hankel functions of the second kind:

$$h_n(\sigma) = j_n(\sigma) - iy_n(\sigma) \tag{1}$$

where $h_n(\sigma)$, $j_n(\sigma)$, and $y_n(\sigma)$ are, respectively, spherical Hankel, Bessel and Neumann functions. Commonly occuring, associated derivative functions, are denoted by

$$H_n(\sigma) = J_n(\sigma) - iY_n(\sigma) \tag{2}$$

where capital letters indicate the differential operation, such as

$$H_n(\sigma) = \frac{1}{\sigma} \frac{d[\sigma h_n(\sigma)]}{d\sigma} \tag{3}$$

Legendre functions are present and denoted by $P_n(\cos\theta)$. To match our notation with others (Grimes, 1982) we also use the modal dependent coefficient D_n, where

$$D_n = \frac{2(2n+1)}{2^n n(n+1)} \frac{n!}{\{[(n-1)/2]!\}^2} \tag{4}$$

With the above definitions, the complete set of Region 1 fields may be written

$$E_r = \sum_{no}^{\infty} n(n+1)\, D_n \beta_n \frac{h_n(\sigma)}{\sigma} P_n(\cos\theta) \tag{5}$$

$$E_\theta = \sum_{no}^{\infty} D_n \beta_n H_n(\sigma) \frac{dP_n(\cos\theta)}{d\theta} \tag{6}$$

$$\eta H_\phi = -i \sum_{no}^{\infty} D_n \beta_n h_n(\sigma) \frac{dP_n(\cos\theta)}{d\theta} \tag{7}$$

where β_n denotes the external field coefficients to be obtained and "no" that n is the set of odd, positive integers.

REGION 2 FIELDS

A complete description of the fields in Region 2 requires a single TEM mode and an infinite set of TM ones.

The TEM voltage and current are, by definition,

$$V(r) = \int_{\psi}^{\pi-\psi} rE_\theta(r,\cos\theta)\, d\theta \tag{8}$$

$$I(r) = 2\pi r\, H_\phi(r,\cos\psi) \tag{9}$$

Boundary Conditions III and IV assure that (8) and (9) remain finite as radius r approaches source radius b, even though the fields E_θ and H_ϕ increase without limit for vanishingly small b.

To describe the TEM mode, it is convenient to introduce the biconical wave admittance, G, where

$$\frac{Gn}{\pi} \ln(\cot\frac{\psi}{2}) = 1 \tag{10}$$

and n is the impedance of space. The admittance Y(r) is

$$Y(r) = \frac{I(r)}{V(r)} \tag{11}$$

In these terms, the input admittance Y_L is

$$Y_L = \frac{I(0)}{V(0)} \tag{12}$$

It follows that

$$V(r) = \frac{V(a)}{G}\{G\cos[k(a-r)] + iY(a)\sin[k(a-r)]\} \tag{13}$$

$$I(r) = V(a)\{Y(a)\cos[k(a-r)] + iG\sin[k(a-r)]\} \tag{14}$$

where Y(a), the terminal admittance, is evaluated at r=a. The input and terminal admittances are related by:

$$Y_L = G\,\frac{Y(a) + iG\tan(ka)}{G + iY(a)\tan(ka)} \tag{15}$$

In these terms, the TEM admittance at each field point is given by

$$Y(r) = G\,\frac{Y_L - iG\tan(kr)}{G - iY_L\tan(kr)} \tag{16}$$

Turning to the TM modes, descriptive Legendre functions are necessarily odd and the functions needed to match Boundary Condition V are of fractional degree. Since fractional degree Legendre functions are of mixed parity, it is convenient to form functions of definite

parity, $M_\nu(\cos\theta)$ and $L_\nu(\cos\theta)$, where:

$$M_\nu(\cos\theta) = [P_\nu(\cos\theta) - P_\nu(-\cos\theta)]/2 \tag{17}$$

$$L_\nu(\cos\theta) = [P_\nu(\cos\theta) + P_\nu(-\cos\theta)]/2 \tag{18}$$

The boundary conditions at the source, r=b, Boundary Conditions III and IV, determine that spherical Neumann functions of positive degree are not present. Incorporating this result, the complete set of fields in Region 2 are described by the following equations:

$$E_r = \sum_\nu \nu(\nu+1)\Upsilon_\nu \frac{j_\nu(\sigma)}{\sigma} M_\nu(\cos\theta) \tag{19}$$

$$E_\theta = \frac{\eta GI(r)}{2\pi rY(r)\sin\theta} + \sum_\nu \Upsilon_\nu J_\nu(\sigma) \frac{dM_\nu(\cos\theta)}{d\theta} \tag{20}$$

$$\eta H_\phi = \frac{\eta I(r)}{2\pi r\sin\theta} - i \sum_\nu \Upsilon_\nu j_\nu(\sigma) \frac{dM_\nu(\cos\theta)}{d\theta} \tag{21}$$

where Υ_ν denotes the internal field coefficients to be obtained and ν the infinite set of real numbers for which $M_\nu(\cos\psi)=0$, in accordance with Boundary Condition V.

SPECIAL FUNCTIONS

Legendre Functions. Legendre functions of the first kind may be expressed in a number of ways. An expansion valid for $0<\theta<\pi$ is (Schelkunoff, 1965)

$$P_\nu(\cos\theta) = \sum_{s=0} \frac{\Gamma(\nu+1+s)}{\Gamma(\nu+1-s)} \frac{(-1)^s}{s!^2} \left[\frac{1-\cos\theta}{2}\right]^s \tag{22}$$

where ν may have either integer or noninteger values. For integer degree functions, ν=n, the series terminates at s=n. Equation (22) is an expansion in powers of $\sin(\theta/2)$.

Two alternative forms found to be useful are:

$$P_n(\cos\theta) = \frac{1}{2^{2n}} \sum_{s=0}^{n} \frac{(2s)!(2n-2s)!}{s!^2(n-s)!^2} \cos(n-2s)\theta \tag{23}$$

$$P_n(\cos\theta) = \sum_{s=0}^{\lfloor n/2 \rfloor} \frac{(-1)^s(2n-2s)!}{2^n s!(n-s)!(n-2s)!} (\cos\theta)^{n-2s} \tag{24}$$

Equation (23) is an expansion in $\cos(n-2s)\theta$, and (24) an expansion in powers of $\cos\theta$; $\lfloor n/2 \rfloor$ indicates the largest integer in $n/2$.

For Eq. (22), in the limit of large values of s the ratio of successive coefficients, say for s=k+1 and s=k, is

$$R = \frac{(\nu+k+1)(k-\nu)}{(k+1)^2} \frac{1-\cos\theta}{2}$$

a ratio that alternates in sign for $\nu>k$. For large values of ν, the ratio is large and the series converges only because the angular term decreases rapidly with s for most angles. As θ approaches 180^o, however, the angular portion approaches unity and the series converges very slowly. Using double precision we terminated the series, whose lead term is equal to one, when successive terms changed results no more than 10^{-16}. For (22) we found that 531 terms were needed at $\theta=150^o$ and about 500,000,000 at 179^o.

Large-angle convergence problems may be avoided by use of a different series. For large angles, we used the expansion (Robin, 1966)

$$P_\nu(\cos\theta) = \sum_{s=0}^{\infty} \frac{(\nu+s)!}{(\nu-s)!(s!)^2} [-\cos^2(\theta/2)]^s \times$$

$$\{\cos\nu\pi + \frac{2}{\pi} \sin\nu\pi \, [\ln \cot(\theta/2) + \Psi(\nu) - \Psi(s)]\} \tag{25}$$

where

$$\Psi(\nu) = \frac{d}{d\nu}(\ln \nu!)$$

This alternative formula for $P_\nu(\cos\theta)$ is an infinite sum with individual terms that decrease as $\cos^2(\theta/2)$, a value much less than one as θ approaches 180^0. This guarentees quick convergence for

large angles.

Boundary Condition V calls for an evaluation of the roots of the function $M_\nu(\cos\theta)$. Figure 2 shows plots of $M_\nu(\cos\theta)$ versus ν for two values of θ, and shows that the function as written contains alternating trivial and desired roots (Badii, 1988). The trivial roots are roots for which the function vanishes for all values of angle; when ν is an even integer the function is equal to zero. We used this property to bracket noninteger roots. The bracket's end points are the integer roots, and inside any bracket there can be at most a single root.

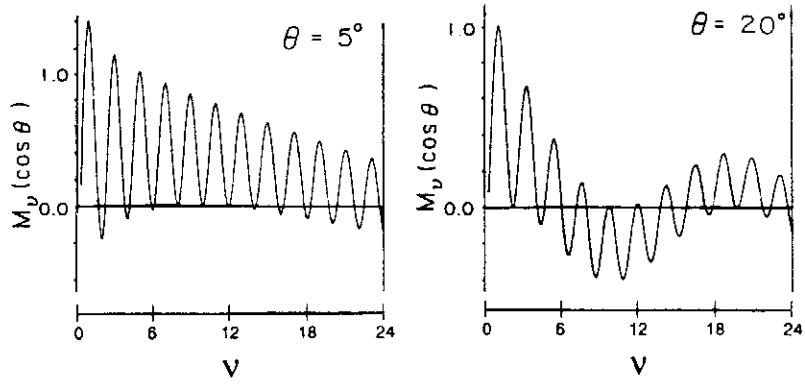

Figure 2. Plots of the antisymmetric Legendre function $M_\nu(\cos\psi)$ as a function of ν for $\psi=5^o$ and $\psi=20^o$, illustrating root positions.

A difficulty was finding a non-integer root very close to an integer one. To remedy the problem, we confined our search to the interval $(2k+\epsilon, 2k+2-\epsilon)$, where k is an integer and ϵ is a "small" number within the tolerance of our computation. This ensures that the determined root is at least ϵ away from a trivial one. The scheme used, outlined elsewhere (Badii, 1988), is a modified *regula falsi* method adapted to our situation. Since the computation was done in quadruple precision, the value of ϵ used was 10^{-30}.

When no root was found in two consecutive intervals the routine

set a flag to indicate the existence of a pair of roots. The integer number in the middle of the interval of length four is assumed to be the root. In addition to bracketing the root, and in order to avoid round-off errors, the search terminates if a new iteration does not change the value of ν. The value of ν at that point is taken to be the root. Table 1 shows the first 16 roots of $M_\nu(\cos 5^o)$.

* * *

Table 1. Values of ν at the first 16 roots of $M_\nu(\cos\theta)$. $\theta=5^o$. The first 11 may be seen from the graphical display of Figure 2.

1.	1.444 484 007 709	9.	18.513 754 995 276
2.	3.609 447 464 872	10.	20.635 248 501 739
3.	5.752 872 182 354	11.	22.756 152 409 445
4.	7.887 328 149 568	12.	24.876 591 378 223
5.	10.016 936 971 261	13.	26.996 657 288 190
6.	12.142 571 291 069	14.	29.116 419 379 140
7.	14.268 228 363 554	15.	31.235 930 827 959
8.	16.391 498 226 300	16.	33.355 233 151 029

* * *

Radial Functions. As noted earlier, Boundary Conditions I and II require use of spherical Hankel functions of the second kind in Region 1 and these require the evaluation of spherical Bessel and Neumann functions. The series used for evaluation are

$$j_\nu(\sigma) = \sum_{s=0}^{\infty} \frac{(-1)^s 2^\nu \Gamma(\nu+s+1)\sigma^{\nu+2s}}{s!\Gamma(2\nu+2s+2)} \tag{26}$$

where ν is either integer or noninteger, and (Grimes, 1986)

$$y_n(\sigma) = -\sum_{s=0}^{n-1} \frac{(2n-2s)!\sigma^{2s-n-1}}{2^n s!(n-s)!} - \sum_{s=0}^{\infty} \frac{(-1)^s s!\sigma^{2s+n-1}}{2^n (2s)!(n+s)!} \tag{27}$$

The radial functions $J_\nu(\sigma)$ and $H_n(\sigma)$ were computed from $j_\nu(\sigma)$ and $h_n(\sigma)$ by using the equalities

$$J_\nu(\sigma) = j_{\nu-1}(\sigma) - \frac{\nu}{\sigma} j_\nu(\sigma) \tag{28}$$

$$H_n(\sigma) = h_{n-1}(\sigma) - \frac{n}{\sigma} h_n(\sigma) \tag{29}$$

PARAMETER DETERMINATION

Linear Equations. The use of Boundary Conditions VI through IX, the integral expressions of Table 2, and the definitions of Table 3 gives the following set of linear equations:

$$n(n+1)D_n\beta_n I_{nn}H_n(ka) = n(n+1)\sum_{\nu}^{\infty} \Upsilon_\nu I_{n\nu}J_\nu(ka) - \frac{\eta GV(a)}{a\pi} P_n(\cos\psi) \tag{30}$$

$$\nu(\nu+1)\Upsilon_\nu I_{\nu\nu}j_\nu(ka) = \sum_{n0}^{\infty} n(n+1)D_n\beta_n I_{n\nu}h_n(ka) \tag{31}$$

$$Y(a) = \frac{2iaG}{V(a)} \sum_{n0}^{\infty} D_n\beta_n h_n(ka)P_n(\cos\psi) \tag{32}$$

Equations (30) and (31) contain both β_n and Υ_ν. They may be combined to give equations involving one coefficient set only:

$$n(n+1)D_n I_{nn}\beta_n h_n(ka)\frac{H_n(ka)}{h_n(ka)} - n(n+1)\sum_{s0}^{\infty} s(s+1)D_s\beta_s h_s(ka) \sum_{\mu}^{\infty} \frac{I_{n\mu}I_{s\mu}}{\mu(\mu+1)I_{\mu\mu}} \frac{J_\mu(ka)}{j_\mu(ka)}$$

$$= -\frac{\eta GV(a)}{\pi a} P_n(\cos\psi) \tag{33}$$

$$\nu(\nu+1)\Upsilon_\nu I_{\nu\nu}j_\nu(ka) - \sum_{\mu}^{\infty} \Upsilon_\mu j_\mu(ka)\frac{J_\mu(ka)}{j_\mu(ka)} \sum_{s0}^{\infty} s(s+1)\frac{I_{s\nu}I_{s\mu}}{I_{ss}} \frac{h_s(ka)}{H_s(ka)}$$

$$= -\frac{\eta GV(a)}{a\pi} \sum_{s0}^{\infty} \frac{I_{s\nu}h_s(ka)}{I_{ss}H_s(ka)} P_s(\cos\psi) \tag{34}$$

Equations (33) and (34) are exact if the running indicies s and μ have no upper bound. For programming purposes, it is necessary to limit both. The programs written for computing β_n and Υ_ν are flexible and can be solved for up to 16 values of n or ν,

Table 2. A Table of Integrals of Legendre functions. $\delta(a,b)$ is the Kronecker delta function of a and b. In all cases, numerical evaluations are made using the right hand side of the equality.

1. $$\int_{\psi}^{\pi-\psi} P_n(\cos\theta)M_\nu(\cos\theta)\,\sin\theta d\theta = I_{n\nu}$$

$$= \frac{2P_n(\cos\psi)}{\nu(\nu+1) - n(n+1)}\,\delta(n,\ \text{odd integer})$$

2. $$\int_{\psi}^{\pi-\psi} M_\nu(\cos\theta)M_\lambda(\cos\theta)\,\sin\theta d\theta = I_{\nu\nu}$$

$$= -\frac{2\sin\psi}{2\nu+1}\,L_{\nu+1}(\cos\psi)\frac{dM_\nu(\cos\psi)}{d\nu}\,\delta(\nu,\lambda)$$

3. $$\int_{0}^{\pi} P_n(\cos\theta)P_m(\cos\theta)\,\sin\theta d\theta = I_{nn}$$

$$= \frac{2}{2n+1}\,\delta(n,m)$$

4. $$\int_{\psi}^{\pi-\psi} \frac{dP_n(\cos\theta)}{d\theta}\,\frac{dM_\nu(\cos\theta)}{d\theta}\,\sin\theta d\theta = n(n+1)I_{n\nu}$$

5. $$\int_{\psi}^{\pi-\psi} \frac{dM_\nu(\cos\theta)}{d\theta}\,\frac{dM_\lambda(\cos\theta)}{d\theta}\,\sin\theta d\theta = \nu(\nu+1)I_{\nu\nu}$$

6. $$\int_{0}^{\pi} \frac{dP_n(\cos\theta)}{d\theta}\,\frac{dP_m(\cos\theta)}{d\theta}\,\sin\theta d\theta = n(n+1)I_{nn}$$

Table 3. Integral expressions used in aperture to match Boundary Conditions VI through IX. Each of the following integrals are evaluated and equated at a^- and a^+.

1. $\int_0^{\infty} d\theta \; E_\theta(\cos\theta)\frac{dP_m(\cos\theta)}{d\theta}$

2. $\int_{\psi}^{\pi-\psi} d\theta \; H_\phi(\cos\theta)\frac{dM_\nu(\cos\theta)}{d\theta}$

3. $\int_{\psi}^{\pi-\psi} d\theta \; H_\phi(\cos\theta)$

* * *

respectively.

Preliminary trials showed that the sequence β_n decreased by many orders of magnitude as n changed from 9 to 31. Since wide range in magnitude of solutions is generally a numerically destabilizing factor, we scaled our unknowns to avoid it.

Equation (33), with the unknown variable x_n defined by

$$x_n = \beta_n h_n(ka) \tag{35}$$

may be written in the form

$$M_n x_n + \sum_{s=0}^{2L-1} N_{ns} x_s = B_n \tag{36}$$

The coefficients of (36) follow by comparison with (33).

There are L unknowns to be determined using (36). Each of the unknowns has coefficient N_{ns}, except for n=s whose coefficient is $M_n + N_{nn}$.

Comparison of (33) and (36) shows that each B_n is proportional to V(a)/a. All field calculations are normalized to

$$V(a) = a \tag{37}$$

Although we desire field evaluation for V(0)=a, it was convenient first to do calculations based upon (37) and then to use (13) to transition to the desired result. Putting V(0)=a in (13) shows that

$$V(a) = \frac{aG}{[G\cos(ka)+iY(a)\sin(ka)]} \tag{38}$$

Initial results, obtained using (37), were multiplied by (38) to shift to the desired normalization.

We take as an example an antenna with parameters ka=2 and $\psi=5^{o}$. In the exterior region, Table 4 shows comparative values of x_n and β_n calculated using 16 terms; the maximum modal number is n=31. Comparison dramatically illustrates the need to use the normalized variable x_n, and not β_n, since the magnitude range of x_n is about 10^3 and that of β_n about 10^{35}. The first two columns of Table 5 shows percentage difference in x_n as calculated using 10 and 16 terms, n=19 and 31 respectively. Generally speaking, the differences are small until the last two terms when they become quite large; we attribute the increase to round off error in the ten term truncation. For our work, we regard the last two terms obtained in this way as being so inaccurate that we do not incorporate their values into subsequent calculations.

In the interior region we assign the symbol u_ν as the unknown variable:

$$u_\nu = \Upsilon_\nu j_\nu(ka) \tag{39}$$

Table 4. x_n and β_n values, Exterior Region, L=16, $\psi=5^o$, ka=2.

Results obtained by solving Equation (33)

n	x_n real	x_n reactive	β_n real	β_n reactive
01	1.006 16 D-01	-1.606 59 D-01	-4.006 65 D-02	-3.367 29 D-01
03	6.202 25 D-02	-1.947 65 D-02	-1.139 27 D-02	-4.224 99 D-02
05	3.193 64 D-02	-1.016 51 D-02	-5.465 19 D-04	-1.717 88 D-03
07	2.138 17 D-02	-7.334 99 D-03	-1.188 71 D-05	-3.456 12 D-05
09	1.574 55 D-02	-5.646 58 D-03	-1.490 30 D-07	-4.155 71 D-07
11	1.214 13 D-02	-4.486 57 D-03	-1.214 57 D-09	-3.286 79 D-09
13	9.588 41 D-03	-3.622 82 D-03	-6.928 71 D-12	-1.833 80 D-11
15	7.657 23 D-03	-2.944 73 D-03	-2.909 29 D-14	-7.565 06 D-14
17	6.129 53 D-03	-2.392 67 D-03	-9.321 03 D-17	-2.387 86 D-16
19	4.882 92 D-03	-1.931 66 D-03	-2.339 71 D-19	-5.914 41 D-19
21	3.843 37 D-03	-1.539 80 D-03	-4.690 39 D-22	-1.170 73 D-21
23	2.963 31 D-03	-1.202 61 D-03	-7.605 64 D-25	-1.874 09 D-24
25	2.210 27 D-03	-9.099 02 D-04	-1.003 12 D-27	-2.436 71 D-27
27	1.560 36 D-03	-6.539 56 D-04	-1.070 19 D-30	-2.553 52 D-30
31	9.937 02 D-04	-4.279 89 D-04	-8.960 27 D-34	-2.080 39 D-33
33	4.885 92 D-04	-2.239 91 D-04	-5.223 96 D-37	-1.139 50 D-36

Table 5. Percentage difference in calculated values of x_n and u_ν between use of L=16 and L=10, $\psi=5^o$, ka=2.

n	x_n real	x_n react	ν	u_ν real	u_ν react
01	0.010	0.101	1.444	-0.808	0.026
03	0.158	0.237	3.609	-0.435	-0.142
05	0.141	0.162	5.753	-0.935	-0.559
07	0.046	0.005	7.887	-1.66	-1.17
09	-0.133	-0.223	10.017	-2.72	-2.10
11	-0.412	-0.572	12.143	-4.36	-3.58
13	-1.14	-1.05	14.268	-7.10	-6.07
15	-1.45	-1.74	16.391	-12.3	-10.9
17	-2.46	-2.83	18.514	-26.5	-24.0
19	-4.40	-4.87	20.635	-194	-181
		*		*	*

and use a linear equation in the form of (36) to solve for the u_ν. Coefficients may be seen by comparison with (34). Table 6 shows comparative values of u_ν and Υ_ν calculated using 16 terms; the maximum modal number is about ν=33.355. The magnitude range in u_ν is about 10^3 and that for Υ_ν about 10^{35}, once again showing the need to use a normalized variable. The last two columns of Table 5 show percentage difference in u_ν as calculated using 10 and 16 terms; about ν=20.635 and 33.355 respectively. In nearly all cases, Region 2 differences are larger than comparative ones of Region 1. Accuracy conclusions parallel those for Region 1.

Table 6. u_ν and Υ_ν values, Interior Region, L=16, $\psi=5^o$, ka=2. Results obtained by solving Equation (34)

ν	u_ν real	u_ν reactive	Υ_ν real	Υ_ν reactive
01.444	+4.338 24 D-02	-1.759 63 D-01	+1.328 36 D-01	-5.387 97 D-01
03.609	+3.681 70 D-02	-2.371 37 D-02	+1.436 44 D-00	-9.252 04 D-01
05.753	+2.233 79 D-02	-1.176 34 D-02	+3.365 07 D+01	-1.772 09 D+01
07.887	+2.599 71 D-02	-1.275 71 D-02	+3.042 73 D+03	-1.493 10 D+03
10.017	-1.083 48 D-01	+5.104 27 D-02	-1.653 06 D+06	+7.787 56 D+05
12.143	-8.896 11 D-03	+4.077 74 D-03	-2.672 94 D+07	+1.225 20 D+07
14.268	-3.574 76 D-03	+1.605 94 D-03	-2.982 97 D+09	+1.340 09 D+09
16.391	-1.950 95 D-03	+8.627 55 D-04	-6.072 22 D+11	+2.685 28 D+11
18.514	-1.244 46 D-03	+5.432 31 D-04	-1.870 69 D+14	+8.165 96 D+13
20.635	-8.803 10 D-04	+3.800 04 D-04	-8.044 03 D+16	+3.472 38 D+16
22.756	-6.740 37 D-04	+2.880 61 D-04	-4.606 46 D+19	+1.968 65 D+19
24.877	-5.520 14 D-04	+2.337 08 D-04	-3.407 56 D+22	+1.442 63 D+22
26.997	-4.814 11 D-04	+2.019 34 D-04	-3.191 58 D+25	+1.338 75 D+25
29.116	-4.482 82 D-04	+1.854 07 D-04	-3.745 88 D+28	+1.555 64 D+28
31.236	-4.525 56 D-04	+1.854 07 D-04	-5.530 85 D+31	+2.265 93 D+31
33.355	-5.311 09 D-04	+2.239 27 D-04	-1.090 87 D+35	+4.599 33 D+34

Separate calculations of x_n and u_ν permit an internal check on consistency, for the u_ν permit calculation of x_n using (30). Simlarly the x_n permit calculation of u_ν using (31). Percentage differences for both using this indirect method are listed in Table 7. Percentage difference with the u_ν is about 0.069% throughout the range, for both real and reactive parts. We consider the agreement to be adequate for our purposes.

Regression Analysis. Still another testing of the values was performed using regression analysis. By this method, instead of direct solution of a linear system the program attempts to minimize a cost function. First we define the individual error "e_n" using Eq. (33) with V(a)=a:

$$e_n = n(n+1)D_n I_{nn}\beta_n h_n(ka)\frac{H_n(ka)}{h_n(ka)} - n(n+1)\sum_{so}^{\infty} s(s+1)D_s\beta_s h_s(ka) \times$$

$$\sum_{\mu}^{\infty} \frac{I_{n\mu}I_{s\mu}}{\mu(\mu+1)I_{\mu\mu}} \frac{J_\mu(ka)}{j_\mu(ka)} + \frac{\eta G}{\pi} P_n(\cos\psi) \qquad (40)$$

We define the cost function J to be minimized as:

$$J(x_1, x_2, \ldots x_{2L-1}) = \sum_{n=1}^{2L-1} e_n^2 \qquad (41)$$

and utilize a routine that minimizes J with respect to the x_n using

Table 7. L=16, $\psi=5^{o}$, ka=2.

Percentage difference in x_n or u_ν between direct solution (DS) of Eq. (33) or (34), and indirect solution (IS) obtained by putting solution of Eq. (34) or (33) in Eq. (30) or (31). Percentages are (100)[(DS)-(IS)]/(DS)

	x			u	
n	real	react	ν	real	react
01	-0.053	+0.015	1.444	0.069	0.069
03	+0.045	-0.028	3.609	0.069	0.069
05	+0.008	-0.069	5.753	0.069	0.069
07	-0.006	-0.077	7.887	0.069	0.069
09	-0.016	-0.069	10.017	0.069	0.069
11	-0.021	-0.069	12.143	0.069	0.069
13	-0.027	-0.069	14.268	0.069	0.069
15	-0.033	-0.069	16.391	0.069	0.069
17	-0.038	-0.069	18.514	0.069	0.069
19	-0.042	-0.069	20.635	0.070	0.069
21	-0.047	-0.069	22.756	0.069	0.069
23	-0.053	-0.069	24.877	0.069	0.069
25	-0.060	-0.069	26.997	0.069	0.069
27	-0.069	-0.069	29.116	0.069	0.069
29	-0.084	-0.069	31.236	0.069	0.070
31	-0.123	-0.070	33.355	0.069	0.086

gradient information, $\partial J/\partial x_n$. The zero vector is used as an initial estimate of x_n. Results are the same as shown in Table 4 for all significant digits. Although this is expected since regression analysis of an L equation, L unknown linear system as outlined should result in the solution found when the L by L system is solved directly, the fact that the sequence x_n converges to the solution sequence shows that the system of linear equations is well conditioned.

BICON2 Program. The FORTRAN program, BICON2, written to generate the tables shown in this section is detailed elsewhere (Badii, 1988). The program computes the unknown parameters and the physical characteristics of the antenna. BICON2 must be supplied with the value of σ and with a field of ψ-dependent constants. This field is produced using program GENER. Roots of $M_\nu(\cos\psi)$, integrals $I_{\nu\nu}$ and $I_{n\nu}$, and other constants may be computed once and then stored for repeated use by BICON2.

BICON2 is dedicated to solving linear equations (33) and (34). One of the subroutines in the IMSL package is used to solve sytems of equations with complex coefficients; this subroutine package is regarded as the best high precision version available at the time (Badii, 1988). It solves the linear system and it performs helpful solution refinements.

As previously discussed, the accuracy of unknowns calculated using up to the highest indices is poor, and therefore we did not use them in the calculations that follow. The computed values of unknowns with lower indices, as illustrated earlier, depend upon the number of terms used in the summations. The solution stabilizes once this number exceeds ten and in all cases we used from twelve to sixteen terms.

In the exterior region, the L=16 term corresponds to modal number 31; in the interior region it depends upon Ψ and for $\Psi=5^{o}$ it is about 33.355, see Table 1. The difficulty with holding numerical accuracy may be seen from the exterior functions. Legendre polynomial $P_{31}(\cos\theta)$ has 31 roots over the angular range of interest. It is an odd, alternating series in powers of $\cos\theta$; the coefficient of the 31st and 23rd powers of $\cos\theta$ are, respectively, about 2 and 150 x 10^{9}. Resulting extreme changes with angle make holding acceptable accuracy with increasing modal number difficult and ultimately not possible; we truncated our work at L=16.

RESULTS

Admittance. Knowledge of the set of β_n permits calculation of terminal admittance Y(a) using Equation (32). In turn, Y(a) and (15) determine the input admittance and/or impedance. Figures 3, 4 and 5 show the resistive and reactive portions of the input impedance as a function of arm length. Figure 3 is for $\Psi=5^{o}$. It illustrates the number of modes needed for accurate impedance values. The long-dash line uses the first mode only. The medium-dash line includes the first three modes, and the short-dash line includes the first six modes. Plots of the first ten modes and the first thirteen modes, shown by the solid line, are not distinguishable. Figures 4 and 5 show the resistive and reactive portions of the input impedance as a function of arm length using thirteen modes, respectively for conic angles $\Psi=1^{o}$ and $\Psi=20^{o}$.

Figure 6 is of special importance for historical reasons (Tai, 1949). It is a plot of inverse radiation impedance, R + jX versus arm length.

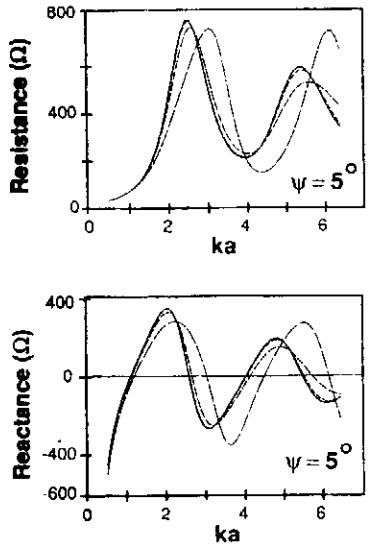

Figure 3. With conic angle $\psi=5^{O}$, plots of input resistance and reactance versus arm length. The long-dash curve uses the first mode only, the medium-dash curve uses the first three modes, the short-dash curve uses the first six modes, and the solid curve uses the first ten modes. The latter curve is indistinguishable from a similar curve using the first thirteen modes.

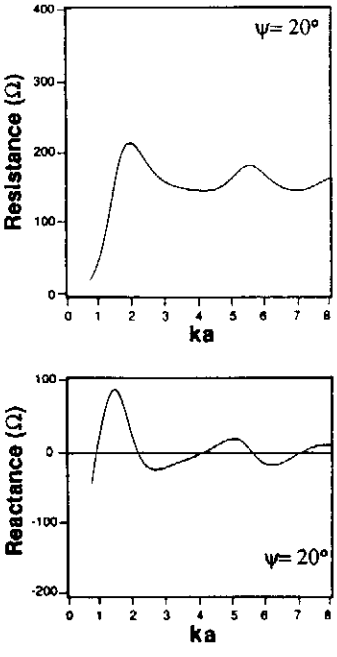

Figure 5. Input impedance with conic angle $\psi=20^{O}$ as a function of normalized arm length ka.

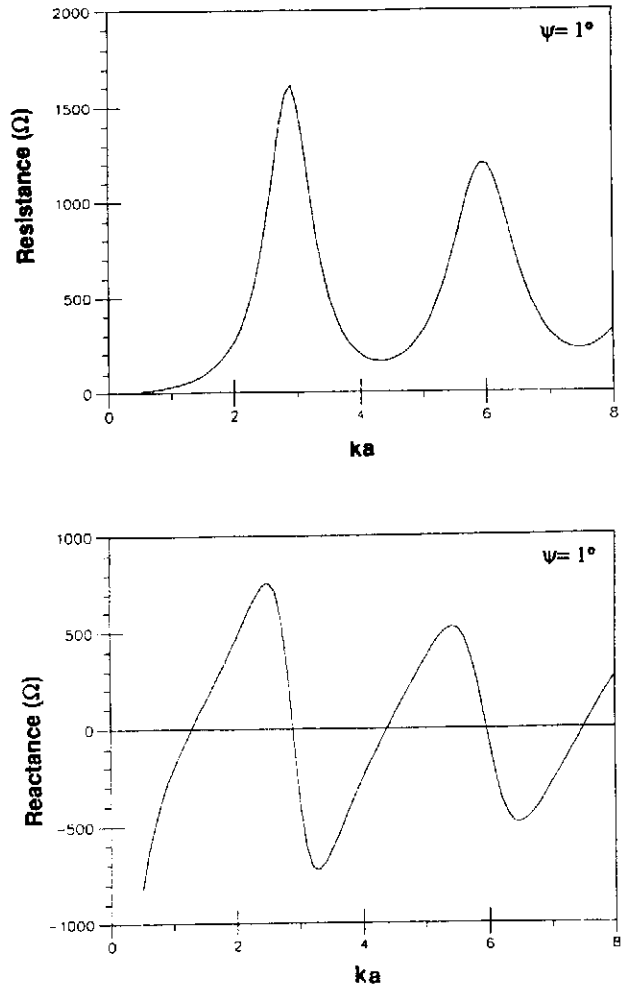

Figure 4 Input impedance with conic angle $\psi= 1^{O}$ as a function of normalized arm length ka.

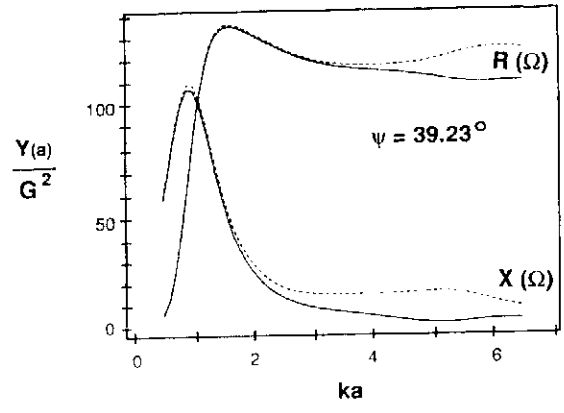

Figure 6 With conic angle $\psi= 39.23^{O}$, plots of inverse radiation impedance versus arm length. The solid curve uses the first mode only. The dashed curve uses seven terms and is indistinguishable from a similar curve using thirteen terms. The dashed curve appears to be in good agreement with Tai's two term curve.

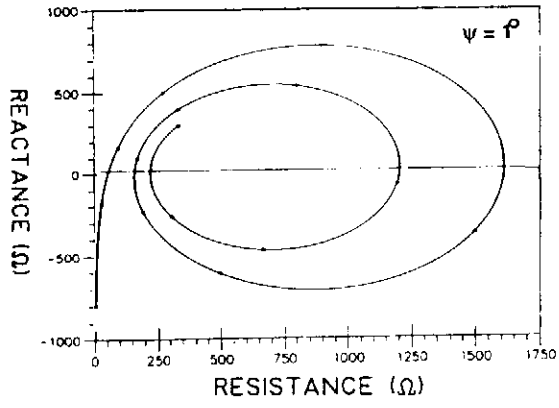

Figure 7. Input impedance for ψ=1°. Asterisks mark ka values from 0.5 through 8.0 in 0.5 unit steps. Real axis crossings are at ka= 1.28, 2.89, 4.39, 5.96, 7.51.

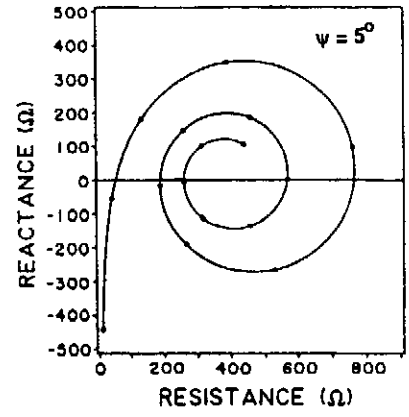

Figure 8. Input impedance for ψ=5°. Asterisks mark ka values from 0.5 through 8.0 in 0.5 unit steps. Real axis crossings are at ka=1.11, 2.59, 4.06, 5.51, 7.14.

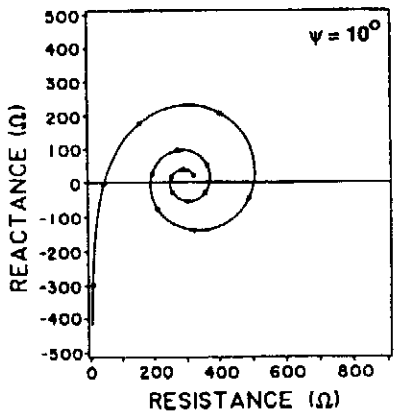

Figure 9. Input impedance for ψ=10°. Asterisks mark ka values from 0.5 through 8.0 in 0.5 unit steps. Real axis crossings are at ka=1.01, 2.41, 3.88, 5.29, 6.83.

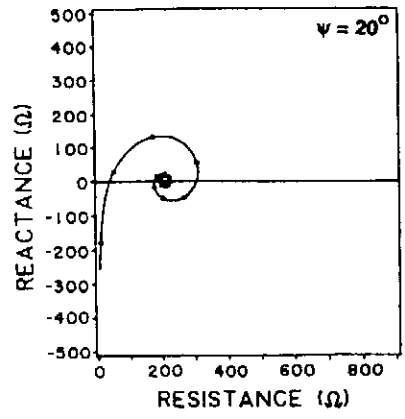

Figure 10. Input impedance for ψ=20°. Asterisks mark ka values from 0.5 through 8.0 in 0.5 unit steps. Real axis crossings are at ka= 0.90, 2.21, 3.73, 5.44, 7.32.

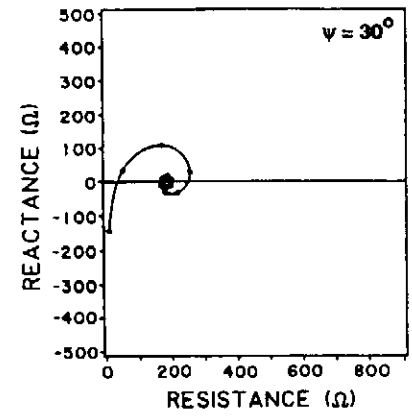

Figure 11. Input impedance for ψ=30°. Asterisks mark ka values from 0.5 through 8.0 in 0.5 unit steps. Real axis crossings are at ka= 0.85, 2.13, 4.09, 5.59, 7.05.

Figures 7 through 11 show the complex impedance versus arm length for five different values of Ψ. In each figure asterisks mark ka values from 0.5 through 8.0 in 0.5 steps. They illustrate the increasing bandwidth with increasing cone angle as well as, in our opinion, increasing the plausibility of numerical results.

The $\Psi=1^{O}$ results are in general agreement with others (Schelkunoff, 1952), (Papas and King, 1949), (Brown and Woodward, 1952), (Bevensee, 1973), (Tai, 1984). Schelkunoff (Schelkunoff, 1952) gives tabular data for the thin antenna case against which we can directly compare; his results are based upon the interior modal numbers being integers. Since integer values are approached only very slowly as Ψ decreases toward zero (Grimes, 1982), we expect and obtain similar shapes with significant differences in detail between very thin and $\Psi=1^{O}$ antennas. Figure 12 shows the inverse radiation impedance ($Y(a)/G^2$) versus antenna arm length for the two cases.

* * *

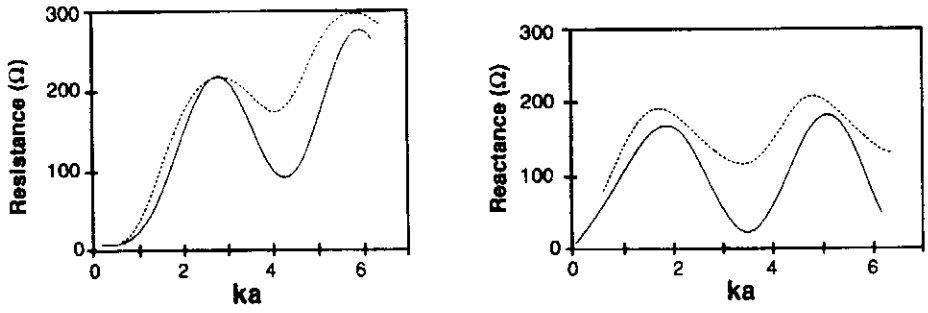

Figure 12. Plots of the inverse radiation impedance, $Y(a)/G^2$, versus antenna arm length. The solid lines represent values computed by Schelkunoff [2, Table V, 180^{O}] for the thin antenna case; the dashed curves show our computations for a 1^{O} cone.

* * *

Surface Current and Charge Density. Knowledge of $H_{\phi}(r,\cos\Psi)$ in Region 2 and $H_{\phi}(a,\cos\theta)$ in Region 1 permits calculation of the surface current density. The currents are

$I_r(r,\Psi) = 2\pi r\sin\Psi\ H_\Phi(r,\cos\Psi)\hat{r}$ on the arms and $I_\theta(a,\theta) = -2\pi a\sin\theta$ $H_\Phi(a,\cos\theta)\hat{\theta}$ on the caps. Since by Boundary Condition VII the magnetic field is continuous through the interface, it follows that

$$I_r(a^-,\Psi) + I_\theta(a,\Psi^-) = 0 \tag{42}$$

An example of current magnitude is shown in Figure 13 for the case $\Psi=5^o$ and ka=1. Sigma values less than ka represent points on the antenna arm in Region 2, and sigma values greater than ka represent points on the caps in Region 1. The glitch shown at kr=ka is due to differences in round off error of the Region 1 and Region 2 solutions. For this antenna, the current decreases monotonically with increasing radius on the antenna arm and across the cap, becoming equal to zero on the axis.

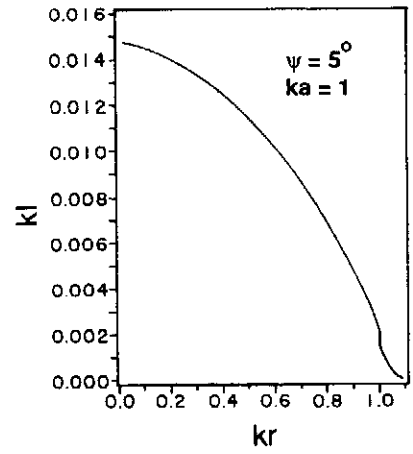

Figure 13. Current magnitude on arm and cap, $\psi=5^o$, ka=1.

Knowledge of normal electric field intensities permits calculation of the surface charge density. Charge per unit length are $Q(r,\Psi) = 2\pi\epsilon r\sin\Psi\ E_\theta(r,\cos\Psi)$ on the arms and, correspondingly, $Q(a,\theta) = 2\pi\epsilon a\sin\theta\ E_r(a,\cos\theta)$ on the caps. Both quantities are plotted in Figure 14 for the special case $\Psi=5^o$ and ka=1. The figure shows that, for this antenna, charge density increases

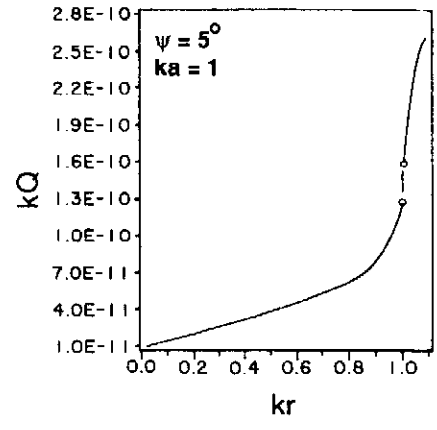

Figure 14. Charge magnitude per unit length on arm and cap, $\psi=5^o$, ka=1.

monotonically with increasing path distance from the origin.

Aperture Fields. Boundary conditions V through IX were applied to obtain the field solutions. A check of the accuracy of the solutions may be made by comparing them across the aperture. Although matching throughout the region is reasonably good, the discontinuity at (a,ψ) makes a match there difficult. We calculated mean square differences both of the angular and the radial electric fields across the interface, as a function of the number of expansion terms used in both Region 1 and Region 2. Best fits were obtained for the combination of 14 and 11 terms in Regions 1 and 2, respectively n=27 and ν=22.756; decreasing accuracy of higher order terms and the additional accuracy obtained from them appear to compensate at these modal values. Figures 15 and 16 show such comparisons for $\psi=5^{o}$ and a=1 using the normalization V(a)=a. Region 2 fields are put equal to zero for $\theta<\psi$. In Region 1 the angular electric field E_{θ} vanishes on the cap but the radial field E_{r} does not.

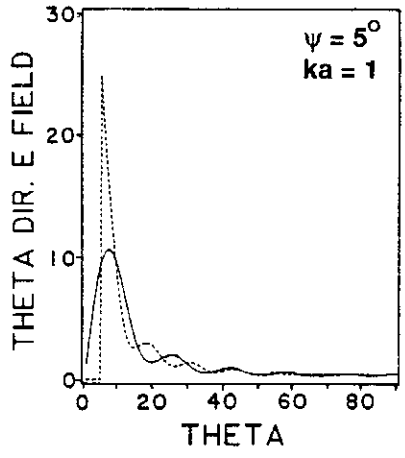

Figure 15. Azimuth electric field in aperture, as calculated. Solid line, Region 1, uses 14 term expansion. Dashed line, Region 2, uses 11 term expansion.

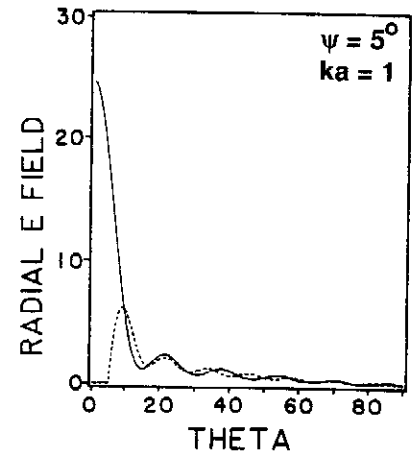

Figure 16. Radial electric field in aperture, as calculated. Solid line, Region 1, uses 14 term expansion. Dashed line, Region 2, uses 11 term expansion.

Average Power. Using the normalization V(a)=a, the average radiated power P_{av} may be calculated from the input parameters as

$$P_{av} = \frac{1}{2} \mathrm{Re}\{V(a)I(a)\} = \frac{a^2}{2} \mathrm{Re}\{Y(a)\} \tag{43}$$

and, using the radiative field in Region 1, from the equation

$$P_{av} = \frac{8\pi}{\eta k^2} \sum_{n=0}^{\infty} \frac{(2n+1)}{n(n+1)} |D_n \beta_n|^2 \tag{44}$$

Plots obtained using the two equations were indistinguishable. Plots of power versus arm length are shown in Figure 17 as a function of ka, for ψ equal to 5^o, 10^o, 20^o, and 30^o; normallization is V(0)=1. There are three sharp resonances at $\psi=5^o$ and one at $\psi=30^o$.

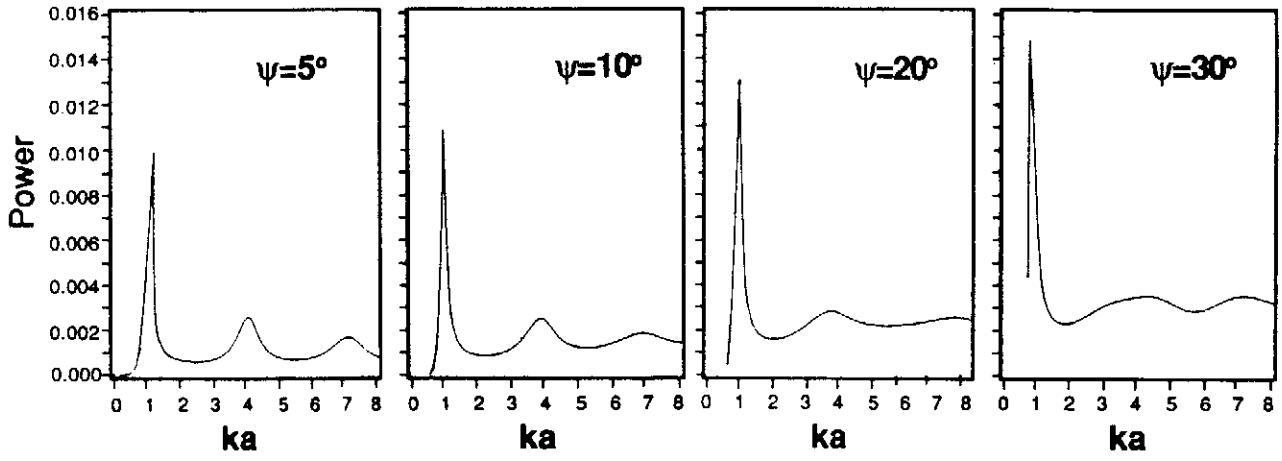

Figure 17. Time average power flow versus normalized arm length ka for constant V(a). Curves obtained by using the far-field expressions or by using the input parameters are indistinguishable. Conic angles are: $\psi=5^o;10^o;20^o;30^o$.

* * *

Radiation Patterns. Region 1 fields may be used to calculate the far field radiation pattern. For our calculations we put

$$h(\sigma) = \frac{i^{n+1}e^{-i\sigma}}{\sigma} \tag{45}$$

then took the product

$$P(\theta) = \frac{1}{2}\,\mathrm{Re}\{E_\theta H_\phi^*\} \tag{46}$$

Results are shown in Figure 18 for an antenna with $\psi=5^o$, and ka taken at each of the first three resonances: ka=1.11, 4.06, and 7.04. In contrast with near field calculations, the series converges rapidly and only the first few values of n are needed. The far field modal field E_θ is proportional to $\sigma\beta_n$ and β_n decreases rapdily with increasing n, see Table 4. Patterns are not distinguishable between three or more modes.

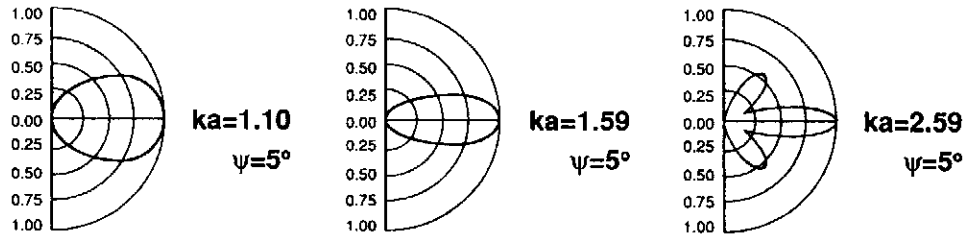

Figure 18. Far field radiation patterns for the first three resonant lengths, $\psi=5^o$. (A), ka=1.10, maximum gain 1.59. (B), ka=2.59, maximum gain 2.17, (C), ka=4.06, gain 2.15 with side lobe maxima at 40^o and 140^o, gain 1.20.

* * *

CONCLUSIONS

A numerical analysis of biconical transmitting antennas is described that, although subject to round-off and truncation errors, is complete from an electromagnetic point of view. Techniques and methods are discussed, detailed, and evaluated. We use the Schelkunoff solution and evaluate all necessary spherical functions, necessarily using a truncated set of field coefficients. Although in

principle all physically possible values of conic angle "Ψ" and arm length "a" may be included, machine accuracies in fact limit useable range. In general, the shorter the arm length the less the number of terms needed for an accurate solution, and the greater the accuracy needed on the largest terms. The shortest length analyzed was ka = 0.4.

The full solution finds the input impedance and all fields, including both near and far ones. From the fields we obtain antenna surface current and charge density, and the radiation field pattern.

The Schelkunoff method applies a conductive-antenna boundary condition to Maxwell's equations, and yields field expressions as sums over an infinite number of linear, z directed, electric multipolar moments: each moment with its own magnitude and phase. The interior region contains a TEM field component and the exterior region does not. Field continuity across the regional interface relates the two sets.

The relative values of field coefficients are determined by values of spherical radial functions and integrals of Legendre functions. A root-finding program was used to obtain the degrees of interior region spherical functions. Methods for numerical computation of Legendre functions with convergence speed-up schemes were found, as were methods for finding integrals over products of Legendre functions. Numerical evaluation of spherical Bessel functions both of integer and noninteger degree were made and are described, as were evaluations of integer degree spherical Hankel fucntions.

Within each coefficient set, the ratio of coefficient magnitudes amongst coefficients important to the solution is very large. With the antenna parameters used the ratio was typically about 10^{35}.

Therefore scaling was needed to stay within a tractable range and to permit stable numerical evaluation. Using this approach, first the parameter sets were obtained by solving the linear equations, then the sensitivity of the coefficients to truncated set size examined. The solution was then verified using linear regression, and results compared. A solution check was made by comparing fields in the two regions at the antenna aperture. All computations were evaluated for several different arm lengths and cone angles.

Input impedance is graphed for several cone angles and arm lengths. Surface currents and charges on the arms and caps are discussed and sketched. Radiated power is shown for several antennas using the voltage and current at the antenna terminals and again using the far field terms; results are indistinguishable. Several radiation patterns are included.

The work emphasizes that the number of terms necessary in the expansion to accurately describe a particular quantity depends upon the quantity. For example, even with keeping 16 terms, that is external Legendre functions through order 31, we cannot accurately obtain the fields near the arm-junction singularity. On the other hand, only the first few terms are needed to accurately describe far field phenomena.

We conclude that this method provides the correct parameter sets and that it may be used with confidence to compute physical properties of transmitting biconical antennas.

REFERENCES

Badii, B. (1988): "Numerical Analysis of the Transmitting Biconical Antenna." Electrical Engineering Doctoral dissertation, The Pennsylvania State University, 1988. Available from University Microfilm, Ann Arbor MI.

Bevensee, R. M. (1973): *Handbook of Conical Antennas and Scatterers*, Gordon and Breach Science Publishers, New York.

Brown, G. H., and O. M. Woodward Jr. (1952): "Experimentally Determined Radiation Characteristics of Conical and Triangular Antennas," RCA Review, vol. 13, pp. 245.

Grimes, D. M. (1982): "Biconcial Receiving Antennas," J. Math. Phys., vol. 23, pp. 897-914.

Grimes, D. M. (1986): "Quantum Theory and Classical, Nonlinear Electronics," Physica, vol. 20D, p. 298.

Papas, C. H., and R. King (1949): "Radiation from Wide-Angle Conical Antennas Fed by a Coaxial Line," Proc. IRE, vol. 39, pp. 1269.

Robin, L. (1966): *Tables Numeriques des Fonctions Associees de Legendre*, Centre National D'etudes des Telecommunications, Paris.

Schelkunoff, S. A. (1946): "Principal and Complementary Waves in Antennas," Proc. IRE, vol. 34, pp. 23-32.

Schelkunoff, S. A. (1952): *Advanced Antenna Theory*, D. Van Nostrand Co. Inc., Princeton, NJ.

Schelkunoff, S. A. (1965): *Applied Mathematics for Engineers and Scientists*, 2nd ed., D. Van Nostrand Co. Inc., Princeton, NJ.

Smith, P. D. P. (1948): "The Conical Dipole of Wide Angle," J. Appl. Phys., vol. 19, pp. 11-23.

Tai, C. T. (1948): "On the Theory of Biconical Antennas," J. Appl. Phys., vol. 19, 1155-1160.

Tai, C. T. (1949): "Application of a Variation Principle to Biconical Antennas," J. Appl. Phys., vol. 20, 1076-1160.

Tai, C. T. (1984): "Dipoles and Monopoles," In Antenna Engineering Handbook, 2nd ed., Edited by R. C. Johnson and H. Jasik, McGraw Hill Book Company, New York, pp. 4-13.

Wait, J. R. (1969): "Electromagnetic Radiation from Conical Structures," In *Antenna Theory*, Part I, Edited by R. E. Collin and F. J. Zucker. McGraw Hill Book Co., New York, pp. 483-499.